Bifurcations leading to summer Arctic sea ice loss

Dorian S. Abbot,[1] Mary Silber,[2,3] and Raymond T. Pierrehumbert[1]

Received 18 January 2011; revised 12 July 2011; accepted 19 July 2011; published 15 October 2011.

[1] There is significant interest in whether there could be a bifurcation, sometimes referred to as a "tipping point," associated with Arctic sea ice loss. A low-order model of Arctic sea ice has recently been proposed and used to argue that a bifurcation associated with summer sea ice loss (the transition from perennial to seasonal ice) is unlikely. Here bifurcations are investigated in a variation of this model that incorporates additional effects, including parameterizations of changes in clouds and heat transport as sea ice is lost. It is shown that bifurcations can separate perennially and seasonally ice-covered states in this model in a robust parameter regime, although smooth loss of summer sea ice is also possible. Hysteresis and jumps associated with bifurcations involving winter sea ice loss are larger than those associated with summer sea ice loss. Finally, in analogy with simulations in global climate models, the low-order model is integrated with time-varying greenhouse gas forcing in both the regime in which summer sea ice is lost via bifurcations and the regime in which it is not. The resulting time series are compared as a preliminary way of investigating ways in which these regimes could be distinguished from each other.

Citation: Abbot, D. S., M. Silber, and R. T. Pierrehumbert (2011), Bifurcations leading to summer Arctic sea ice loss, *J. Geophys. Res.*, *116*, D19120, doi:10.1029/2011JD015653.

1. Introduction

[2] Sea ice, a critical determinant of Arctic climate and ecosystems [*McBean et al.*, 2005], is currently being lost at a rapid rate [*Fetterer et al.*, 2002]. There has been speculation that Arctic sea ice might experience a "tipping point" leading to rapid sea ice loss at some point in the future [e.g., *Lindsay and Zhang*, 2005]. One way that a system can undergo a tipping point with a slow variation in external forcing is to pass through a saddle node bifurcation. Saddle node bifurcations occur when a stable fixed point and an unstable fixed point of a system appear or disappear in tandem as a control parameter is varied [*Strogatz*, 1994]. In the case of Arctic sea ice, a fixed point corresponds to an equilibrium solution of the yearly cycle of ice growth and retreat. If a system exists in a stable fixed point that disappears through a saddle node bifurcation, it must transition violently to another fixed point or other attractor of the system that is not necessarily nearby, so that the bifurcation represents a type of tipping point. The small ice cap instability, which has been described extensively in energy balance models [*North*, 1975, 1984], represents an example of a saddle node bifurcation that leads to tipping point behavior.

[3] *Eisenman and Wettlaufer* [2009, hereinafter EW09] proposed an elegant conceptual mathematical model which reduces the complexities of Arctic sea ice to an ordinary differential equation forced by the seasonal cycle. While such a model is perhaps not useful for making specific predictions, it serves as a useful source of insight into qualitative behavior of the system. EW09 argued that as greenhouse gas levels increase, the transition from a perennially ice-covered Arctic to a seasonally ice-covered Arctic (i.e., loss of summer sea ice) should be smooth, without a bifurcation. Only when greenhouse gas levels are further increased does the system undergo a saddle node bifurcation leading to an abrupt transition to perennially ice-free conditions (i.e., loss of winter sea ice).

[4] On the other hand, *Merryfield et al.* [2008] developed a low-order stochastic difference equation model involving a mapping between summer sea ice extent and winter ice thickness, which they could parameterize to produce results similar to the global climate model (GCM) analyzed by *Holland et al.* [2006], and found bifurcations in it as summer sea ice was lost in a physically relevant parameter regime. This raises the question of whether bifurcations are possible as summer sea ice is lost in the EW09 model, or whether there is something about the EW09 model that prevents such behavior. Additionally, it is possible that processes that are neglected by EW09, but might be important, could be implicitly included by *Merryfield et al.* [2008] since they tune their parameters to GCM results.

[5] Changes in clouds and ocean heat transport as sea ice is lost are potentially important effects that, as EW09 noted, their model does not include. As sea ice is lost, cloud cover, optical properties, and height can change [*Schweiger et al.*,

[1]Department of Geophysical Sciences, University of Chicago, Chicago, Illinois, USA.
[2]Department of Engineering Sciences and Applied Mathematics, Northwestern University, Evanston, Illinois, USA.
[3]Northwestern Institute on Complex Systems, Northwestern University, Evanston, Illinois, USA.

0148-0227/11/2011JD015653

Table 1. Definition of Parameters Used in the Text[a]

Parameter	Definition	Standard Value
α_i	TOA[b] albedo over sea ice	—
α_o	cloud-free TOA[b] albedo over ocean	0.1
$\Delta\alpha_c$	increase in TOA[b] albedo over ocean due to clouds	—
A_0	offset of linearization of Lord versus T	225 W m^{-2}
B	slope of linearization of OLR[c] versus T	2.2 W m^{-2} K^{-1}
ΔA_{ghg}	decrease in OLR[c] due to increased GHG[d] levels	— W m^{-2}
ΔA_c	decrease in A over ocean due to clouds	— W m^{-2}
$F_s(t)$	time-varying TOA[b] insolation	(variable) W m^{-2}
F_{south}	atmospheric heat transport convergence	100 W m^{-2}
F_b	ocean heat transport convergence	2 W m^{-2}
ν	fractional sea ice export per year	0.1 yr^{-1}
C_s	ocean heat capacity per unit surface area	6.3 W yr m^{-2} K^{-1}
k_i	ice thermal diffusivity	2 W m^{-1} K^{-1}
L_i	latent heat of fusion of ice	9.5 W yr W m^{-3}
h_a	ocean-ice parameter transition thickness	0.5 m

[a]A standard value is given or the values used are described in the text.
[b]Top of atmosphere.
[c]Outgoing longwave radiation.
[d]Greenhouse gas.

2008; *Vavrus et al.*, 2009; *Kay and Gettelman*, 2009]. If increased moisture leads to increased cloud albedo, this can retard sea ice loss [*Kay et al.*, 2008; *Vavrus et al.*, 2009]. If increased moisture leads to increased cloud optical thickness, this warms the surface and accelerates sea ice loss [*Vavrus et al.*, 2009; *Abbot et al.*, 2009a]. Similarly, the retreat of sea ice could lead to changes in heat transport into the Arctic, such as the further extension of warm ocean currents into the Arctic basin [*Bitz et al.*, 2006; *Holland et al.*, 2006].

[6] The main purpose of this paper is to investigate the possible effects of changes in clouds with sea ice loss in a low-order model similar to the model by EW09. Our formulation allows the consideration of changes in atmospheric and ocean heat transport as sea ice is lost as well. We find three distinct bifurcation scenarios as greenhouse gas levels are increased. In addition to the behavior found by EW09, we find a robust region of parameter space in which a new seasonal ice state is introduced via a pair of saddle node bifurcations and a region of parameter space in which the only stable states are perennially ice covered and perennially ice free.

[7] The plan of this paper is as follows. In section 2 we describe the low-order model used in this paper, which is a reformulation and extension of the EW09 model. In section 3 we describe the methodology we use to estimate parameters that control the effects of changes in clouds as sea ice is lost in our low-order model from global climate model output and reanalysis product. In section 4 we describe our main results from the low-order model and in section 5 we integrate the low-order model with time-varying greenhouse gas forcing as an exploratory inquiry into the methods that might be used to detect bifurcations associated with summer sea ice loss in more complex models and observations. We discuss our results and conclude in section 6.

2. Low-Order Model

[8] Following EW09, we consider a horizontally averaged column model of the Arctic and use the energy per unit surface area relative to a mixed layer ocean at the freezing point (E) as the state variable,

$$E = \begin{cases} -L_i h_i & E < 0 \\ C_s T & E \geq 0 \end{cases}. \tag{1}$$

Here T is the surface temperature above freezing in Celsius and h_i is the ice thickness (see Table 1 for parameter values).

[9] We derive the model by assuming heat flux balance at the top of the atmosphere and negligible atmospheric heat capacity. This leads to the equation

$$\frac{dE}{dt} = (1 - \alpha(E))F_s(t) - A(E) - BT(E,t) + \Delta A_{ghg} + \nu\mathcal{R}(-E). \tag{2}$$

$F_s(t)$ is the seasonally dependent insolation cycle averaged north of 70.0°N, calculated using the code of *Huybers and Eisenman* [2006]. $A(E) + BT(E, t)$, which we describe in detail below, is a heat loss term that represents the linearized infrared radiation to space minus heat transport into the Arctic. ΔA_{ghg}, which will be our bifurcation parameter, represents the reduction in outgoing longwave radiation due to increased greenhouse gas levels. ν is the fraction of sea ice pushed by wind out of the Arctic each year. $\mathcal{R}(-E)$ ensures this term is zero when there is no sea ice, where

$$\mathcal{R}(x) = \begin{cases} 0 & x < 0 \\ x & x \geq 0 \end{cases}. \tag{3}$$

The model top-of-atmosphere albedo, $\alpha(E)$, varies smoothly from an ice-covered value (α_i) to an ice-free value ($\alpha_o + \Delta\alpha_c$) as E increases through zero. α_i represents the top-of-atmosphere albedo when there is sea ice, including surface albedo, atmospheric scattering, and clouds. α_o represents the clear-sky top-of-atmosphere albedo when there is no sea ice, and $\Delta\alpha_c$ is the increase in top-of-atmosphere albedo due to cloud cover (relative to clear sky) when there is no sea ice. The albedo transition happens over a characteristic energy scale ($L_i h_a$), which represents the fact that when the

Arctic average energy is near zero, there will likely be some ice-covered and some ice-free regions. h_a can therefore be thought of as a measure of the spatial uniformity of Arctic sea ice loss. Specifically, we take

$$\alpha(E) = \frac{\alpha_o + \Delta\alpha_c + \alpha_i}{2} + \frac{\alpha_o + \Delta\alpha_c - \alpha_i}{2}\tanh\left(\frac{E}{L_i h_a}\right). \quad (4)$$

[10] The heat loss term ($A(E) + BT(E, t)$) is reduced by the atmospheric (F_{south}) and oceanic (F_b) heat flux convergence into the Arctic. We also include a reduction in the heat loss term, ΔA_c, as sea ice is lost (as the system crosses $E = 0$). We will primarily think of ΔA_c as representing the decrease in outgoing longwave radiation due to an increase in cloud cover when sea ice is lost. In the introduction we motivated the potential for changes in cloud cover as sea ice is lost through a direct and local feedback. If changes in cloud cover, and therefore outgoing longwave radiation, associated with sea ice loss were instead caused by nonlocal effects such as the rearrangement in the Ferrel and polar cells, the implementation of this effect in the model would be the same. Within the framework of this model it is also possible to use ΔA_c to consider changes in heat transport into the Arctic upon the removal of sea ice, although we will not consider this point further in this paper. Specifically, we take

$$A(E) = A_0 - F_{south} - F_b - \frac{\Delta A_c}{2}\left(1 + \tanh\left(\frac{E}{L_i h_a}\right)\right). \quad (5)$$

For simplicity, we assume the same transition energy scale ($L_i h_a$) for ΔA_c as for $\Delta\alpha_c$. This assumption is reasonable insofar as h_a mainly represents the spatial heterogeneity of sea ice loss. We calculate A_0 and B using the radiative-convective model described by *Pierrehumbert* [2002] run with a surface temperature of 0°C, CO_2 = 400 ppm, and assuming a moist adiabatic profile with a relative humidity of 100%. We note that B represents the climate sensitivity parameter, including the Planck and water vapor feedbacks, but not cloud feedbacks, familiar from other studies [e.g., *Soden and Held*, 2006]. Changes in A_0 due to variations in greenhouse gas levels are represented by ΔA_{ghg}. The small changes in B with respect to greenhouse gas levels are neglected in our model. We discuss the appropriate value for B further in section 3.

[11] Following EW09, when ice is not melting we calculate the surface temperature, T, from surface energy balance, including diffusion of heat from the ice interior to the ice surface, assuming a linear temperature profile in the ice. If the ice is melting at the top we set $T = 0$ and if there is no ice we use equation (1). To summarize,

$$T(E,t) = \begin{cases} -\mathcal{R}\left[\frac{(1-\alpha(E))F_s(t) - A(E) + \Delta A_{ghg} + F_b}{k_i L_i / E - B}\right] & E < 0 \\ \frac{E}{C_s} & E \geq 0 \end{cases}, \quad (6)$$

where $\mathcal{R}(x)$ is the ramp function defined by equation (3).

[12] Our model differs from the model by EW09 in the following important ways:

[13] 1. The EW09 model contains assumptions about the seasonal cycle of cloud albedo, cloud emissivity, and surface fluxes that are drawn from modern observations in the perennially ice-covered Arctic. Since these assumed seasonal cycles are likely inappropriate in a seasonally or fully ice-free Arctic, we remove them here.

[14] 2. We add a state dependence to $A(E)$.

3. Use of GCM Output and Reanalysis Product

[15] Here we describe the way in which we estimate ΔA_c, α_i, and $\Delta\alpha_c$ from reanalysis product (model interpolation of data collected by satellites, weather balloons, and surface-based observations) and a global climate model. We will use these estimates below to motivate which region of low-order model parameter space may be relevant. Given the large gap in complexity between the low-order model and either reanalysis product or a global climate model, however, these estimates should not be viewed as a way to specifically constrain future sea ice behavior based on the low-order model.

[16] The reanalysis product we use is that of the National Centers for Environmental Prediction/National Center for Atmospheric Research (NCEP/NCAR) [*Kalnay et al.*, 1996] and the global climate model we use is the National Center for Atmospheric Research Community Atmosphere Model (CAM) v3.1. The CAM simulations were performed at T42 resolution (2.8° × 2.8°) with a slab ocean with modern specified ocean heat flux run at CO_2 = 280 ppm (runs described by *Abbot et al.* [2009b]). We use 10 years of output from both CAM and NCEP/NCAR to calculate analogs of relevant parameters of the low-order model. We use monthly output because relationships between variables in the low-order model are meant to represent time-averaged, rather than instantaneous, behavior. Since we are trying to determine the ice-free and ice-covered end-members, we only consider variables when the ice fraction is either zero or one here. In the low-order model we interpolate between these end-members, to consider a partially ice-covered Arctic, using equations (4) and (5).

[17] Figure 1 contains a scatterplot of monthly mean values of outgoing longwave radiation (OLR) versus surface temperature (TS) for ocean grid points north of 60°N in CAM and NCEP/NCAR for temperatures ranging from −10°C to 10°C. Only grid points with an ice fraction of zero are plotted for TS greater than 0°C and only grid points with an ice fraction of one are plotted for TS less than 0°C. Two salient observations can be made about the change in OLR as a function of TS when sea ice is removed. First, the variability in OLR for a given TS is much larger when there is no sea ice than when there is sea ice (Figure 1). Second, the typical OLR for a given TS is significantly reduced in the ice-free situation relative to the ice-covered situation. This can be seen from the difference between the values of the lines of best fit of OLR vs. TS at TS = 0 in Figure 1. We note that these differences are statistical in nature and can only be discerned after averaging over long data sets to remove weather noise. Although we do not directly diagnose cloud effects on OLR here, we interpret both of these important characteristics of the OLR versus TS plots as resulting from an increase in cloud cover when sea ice is lost. It is difficult to imagine anything other than clouds that could reduce the OLR by $\mathcal{O}$ (80 W m^{-2}) at a given TS. Also, since clouds are inherently variable, they naturally explain the large observed scatter when there is no sea ice.

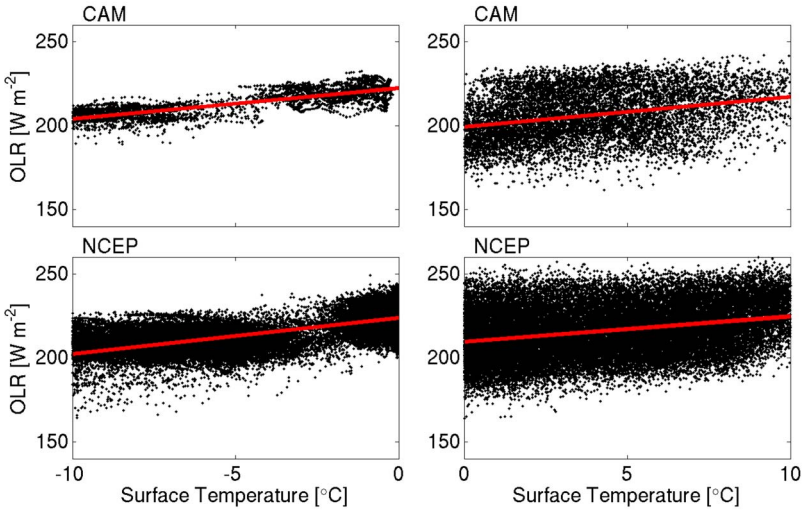

Figure 1. Scatterplot of monthly mean values of outgoing longwave radiation versus surface temperature for ocean grid points north of 60°N in (top) the Community Atmosphere Model (CAM) atmospheric general circulation model and (bottom) the National Centers for Environmental Prediction/National Center for Atmospheric Research (NCEP/NCAR) reanalysis data product. Lines of best fit for both the (left) ice-covered region and (right) the ice-free region are plotted in red.

[18] If we interpret the change in the behavior of OLR as sea ice is lost as being largely due to changes in clouds, then the reduction in the typical OLR for a given TS is due specifically to increased typical cloud optical thickness when sea ice is removed. The parameter ΔA_c in the low-order model represents the decrease in OLR due to increased cloud optical thickness upon the removal of sea ice. To calculate ΔA_c we first calculate the line of best fit for the outgoing longwave radiation over open ocean as a function of surface temperature ($OLR_{ocn} = A_{ocn} + B_{ocn}T_{ocn}$) for $0°C < T_{ocn} < 10°C$ and for outgoing longwave radiation over sea ice as a function of surface temperature ($OLR_{ice} = A_{ice} + B_{ice}T_{ice}$) for $-10°C < T_{ice} < 0°C$. We then let $\Delta A_c = A_{ocn} - A_{ice}$. For CAM we find $\Delta A_c = 23.0$ W m^{-2} and for NCEP/NCAR we find $\Delta A_c = 14.4$ W m^{-2}.

[19] This methodology also allows us to compare the value of B (2.2 W m^{-2}K^{-1}) we calculated above using a radiative convective model to B_{ice} and B_{ocn} from CAM and NCEP/NCAR. For NCEP/NCAR $B_{ice} = 2.2$ W m^{-2} K^{-1} and $B_{ocn} = 1.5$ W m^{-2} K^{-1}. For CAM $B_{ice} = B_{ocn} = 1.8$ W m^{-2} K^{-1}. This suggests that our calculated B is a reasonable value compared to that calculated from CAM and NCEP/NCAR. Detailed investigation of variations in B is beyond the scope of the current work, however, preliminary investigation suggests that modifying B on the order of the variations seen in CAM and NCEP/NCAR does not alter our main conclusions.

[20] We calculate top-of-atmosphere albedos using ocean grid points north of 60°N for which the top-of-atmosphere insolation exceeds 50 W m^{-2}. Probability distribution functions for CAM and NCEP/NCAR albedo in ice-free and ice-covered Arctic regions are shown in Figure 2. The standard deviation is larger in the ice-free than ice-covered distributions. We interpret this as resulting (1) from more cloud cover in the ice-free case, since clouds are inherently variable, and (2) from the lower surface albedo when there is no ice, so clouds have a larger effect on the top-of-atmosphere albedo than when there is ice. The bimodal distribution in the NCEP/NCAR ice-covered albedo distribution is due to a rapid transition from high-albedo fresh snow to lower-albedo snow and ice during late spring and early summer. Based on the means of these distributions we

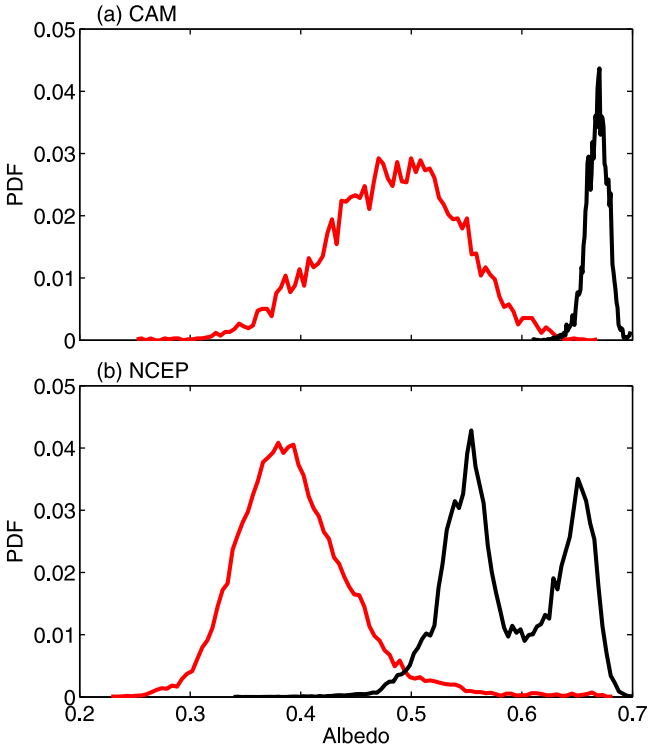

Figure 2. Probability distribution function of the top-of-atmosphere albedo in (a) CAM and (b) NCEP/NCAR for ocean north of 60°N over ice-covered (black) and ice-free (red) regions.

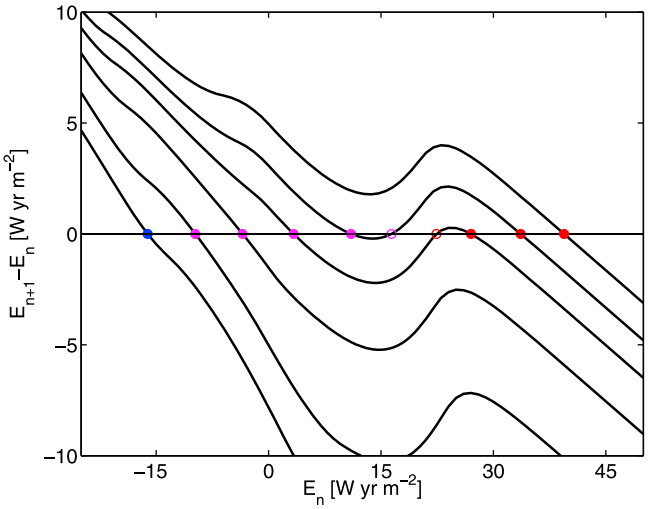

Figure 3. Poincaré map produced by integrating equation (2) for 1 year, from 1 January, for a range of initial conditions (E_n) with $\Delta\alpha_c = 0.3$ and $\Delta A_c = 0$ W m^{-2}. Fixed points of the Poincaré map, which intersect the $E_{n+1} - E_n = 0$ line and correspond to periodic solutions with the same periodicity as the forcing (i.e., annual), are depicted as circles here. Fixed points that are perennially ice covered are colored blue, seasonal ice fixed points are colored magenta, and ice-free fixed points are colored red. Filled circles represent stable fixed points, and open circles represent unstable fixed points. ΔA_{ghg} = 10, 15, 20, 23, 25, and 27 W m^{-2} for the lines plotted here (from bottom to top). In all cases, $\alpha_i = 0.6$ and $h_a = 0.5$ m.

calculate $\alpha_i = 0.67$ and $\alpha_o + \Delta\alpha_c = 0.48$ in CAM and $\alpha_i = 0.59$ and $\alpha_o + \Delta\alpha_c = 0.40$ in NCEP/NCAR. We assume $\alpha_o = 0.1$ in both CAM and NCEP/NCAR in order to calculate $\Delta\alpha_c$ below.

4. Results From Low-Order Model

[21] To study behavior in the low-order model we construct Poincaré maps, which indicate the change in energy from 1 January in one year (E_n) to 1 January in the next year ($E_{n+1} = f(E_n)$) for a range of initial energies. Fixed points (E_n^*) of the Poincaré map occur when $E_{n+1} = f(E_n^*) = E_n^*$ and correspond to periodic solutions of the system with the same periodicity as the forcing (i.e., annual). Fixed points of a Poincaré map are stable for $|f'(E_n^*)| < 1$ and unstable for $|f'(E_n^*)| > 1$ (see *Strogatz* [1994], for more detail). Bifurcations in the system occur when $|f'(E_n^*)| = 1$ and cause the number and/or stability of fixed points to change. Due to the low dimensionality of the low-order model we expect only saddle node bifurcations in it. Saddle node bifurcations occur when pairs of stable and unstable fixed points either appear or disappear as the control parameter (ΔA_{ghg}) is varied. In this section we will use Poincaré maps to determine the locations of saddle node bifurcations that occur as ΔA_{ghg} is increased. We will plot $f(E_n) - E_n$, rather than $f(E_n)$, as a function of E_n so that the fixed points and behavior of $f(E_n)$ are more clear in the diagrams.

[22] When $\Delta\alpha_c$ (equation (4)) is large and ΔA_c (equation (5)) is small, a smooth transition from perennial to seasonal sea ice occurs in our model and there are a total of two saddle node bifurcations as ΔA_{ghg} is increased. The first saddle node bifurcation creates the stable ice-free state, while the second one destroys the stable seasonal ice state (Figure 3). This is consistent with the results of EW09. For lower $\Delta\alpha_c$ or higher ΔA_c, two additional saddle node bifurcations occur, so that there are a total of four bifurcations as ΔA_{ghg} is increased, indicating qualitatively different behavior (Figure 4a). These additional saddle node bifurcations create and destroy a new stable seasonal ice state that is not a smooth continuation of the perennial ice state. For even lower $\Delta\alpha_c$ or even higher ΔA_c, the additional stable seasonal ice state and the two intermediate saddle node bifurcations associated with it vanish (Figure 4b). There is usually no stable seasonal ice state in this regime, although for larger values of h_a than that used for Figure 4b, the perennial ice state sometimes transitions to a tenuous seasonal ice state in a very narrow ΔA_{ghg} range just before it is lost in a saddle node bifurcation. Notice that the behavior of the EW09 model is not recovered in our model by setting $\Delta\alpha_c = \Delta A_c = 0$. This is primarily due to the fact that EW09 use $\alpha_o + \Delta\alpha_c = 0.2$, or $\Delta\alpha_c \approx 0.1$, although because of slight differences in the formulation of the two models we would not have expected exact correspondence.

[23] The physical interpretation of the effect of $\Delta\alpha_c$ and ΔA_c on the model is as follows. A high cloud albedo when sea ice is lost (large $\Delta\alpha_c$) makes the albedo similar before

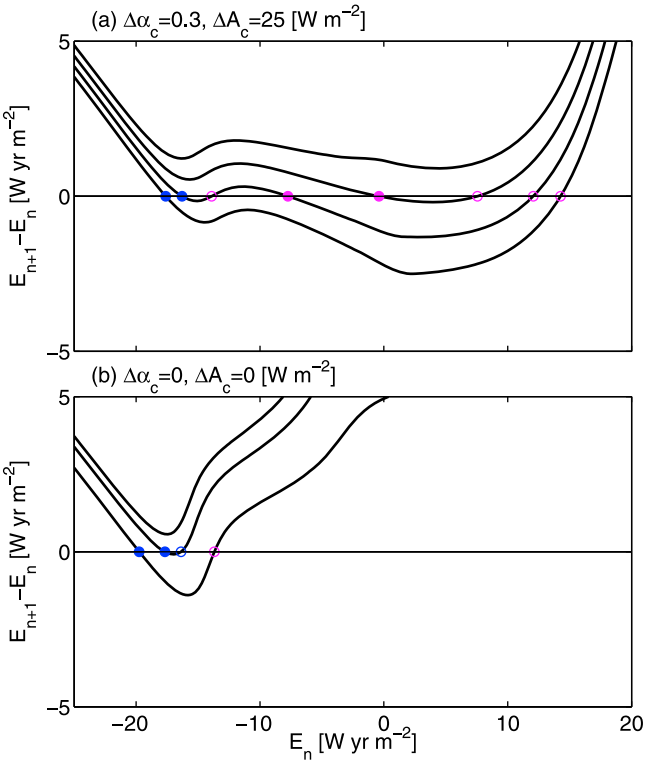

Figure 4. As in Figure 3 but with (a) $\Delta\alpha_c = 0.3$ and $\Delta A_c = 25$ W m^{-2} and (b) $\Delta\alpha_c = 0$ and $\Delta A_c = 0$ W m^{-2}. ΔA_{ghg} = 7.5, 8.5, 9.5, and 10.5 W m^{-2} for the lines plotted in Figure 4a, and ΔA_{ghg} = 4, 6, and 7 W m^{-2} for the lines plotted in Figure 4b. Notice that the E_n range is restricted relative to Figure 3 here. An ice-free state exists for higher E_n in all cases.

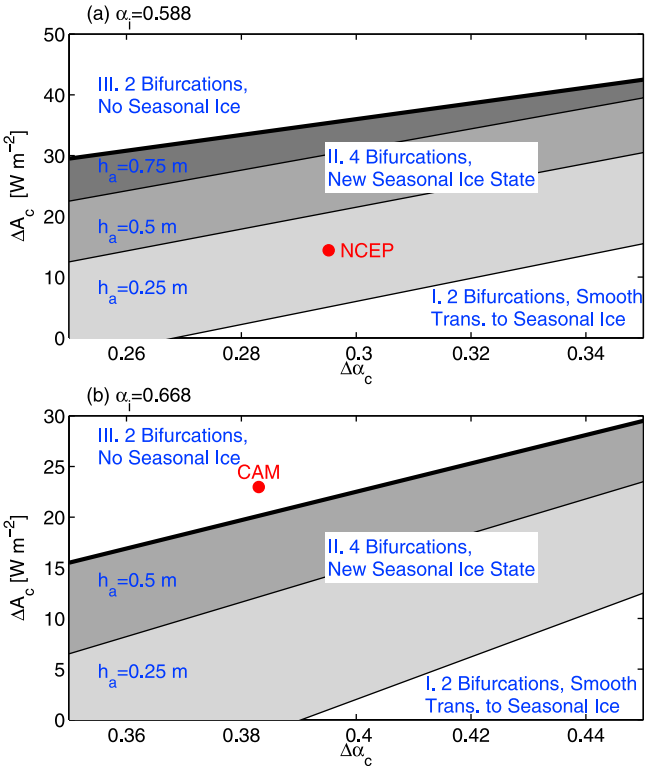

Figure 5. Diagram showing the range in the ($\Delta\alpha_c$, ΔA_c) parameter plane for which the low-order model exhibits the following types of behavior as ΔA_{ghg} is increased: region I includes two bifurcations and a smooth transition from perennial to seasonal ice (EW09 and Figure 3), region II includes four bifurcations with a new stable seasonal ice state created and destroyed by two of these bifurcations (Figure 4a), and region III includes two bifurcations and no seasonal ice state (Figure 4b) or a fragile seasonal ice state that exists in a very narrow ΔA_{ghg} range (see text). The shaded regions reflect the size of region II for different values of h_a. The thick black line separates regions II and III and does not depend on h_a to within 1.0 W m^{-2} in ΔA_c. Since the thick black line is the upper bound on region II for all h_a, region II for h_a = 0.25 m includes region II for h_a = 0.5 and 0.75 m and so forth. (a) The ice albedo, α_i, is set to its value calculated from the NCEP/NCAR reanalysis data set, and the red circle shows ($\Delta\alpha_c$, ΔA_c) for this data set. (b) Region II for h_a = 0.75 m has a width of 1.0 W m^{-2} or less in ΔA_c, so it is not plotted. In Figure 5b, α_i is set to its value estimated from the CAM global climate model, and the red circle shows ($\Delta\alpha_c$, ΔA_c) for CAM.

and after sea ice loss, which tends to reduce nonlinear behavior and stabilize the system. This promotes a smooth transition from perennial to seasonal sea ice. As $\Delta\alpha_c$ is decreased, however, the system becomes more nonlinear so that the transition to a seasonal ice state occurs via a saddle node bifurcation. If $\Delta\alpha_c$ is decreased even more the loss of ice leads to such a large increase in absorbed solar radiation that no stable seasonal ice state can exist. An increase in the atmospheric optical thickness due to increased clouds as sea ice is lost, captured by the parameter ΔA_c, causes a warming that has effects that parallel a decrease in $\Delta\alpha_c$.

[24] The physically similar consequences between decreases in $\Delta\alpha_c$ and increases in ΔA_c are reflected in the model by the way that lines of approximately constant slope divide regions of behavior in the ($\Delta\alpha_c$, ΔA_c) parameter plane (Figure 5, see Appendix A for a mathematical derivation of one of these lines). In Figure 5 we map behavior for two different values of α_i which, along with $\Delta\alpha_c$ and ΔA_c, we estimate from CAM and NCEP/NCAR. The size of the region of the ($\Delta\alpha_c$, ΔA_c) plane in which the model exhibits four bifurcations is highly dependent on h_a (see, e.g., Figure 6), the transition sharpness parameter, expanding as the transition from ice to ice-free parameters becomes sharper with respect to E (Figure 5). For the value of h_a used by EW09 and in Figures 3 and 4, and for lower h_a, this region is broad.

[25] Comparison with the reanalysis and GCM data indicates that the portion of parameter space in which four bifurcations occur (region II, see Figure 4a) or no seasonal ice state is possible (region III, see Figure 4b) may be physically accessible (Figure 5). Given the uncertainty in determining appropriate values for parameters in the low-order model (section 3), we view this as an indication that the behavior depicted in Figure 4 may be relevant for future sea ice, rather than a specific prediction of future sea ice behavior. For example, we note our methodology puts CAM barely in region I, where no seasonal sea ice state is possible, despite the fact that it is the atmospheric component of Community Climate System Model version 3 (CCSM3), which exhibits seasonal sea ice in transient experiments [e.g., *Wang and Overland*, 2009].

5. Time-Varying Greenhouse Gas Forcing

[26] We have uncovered robust, physically pertinent parameter regimes of the low-order model where bifurcations lead to summer sea ice loss. The hysteresis loops and energy jumps associated with summer sea ice loss, however, are smaller than those associated with winter sea ice loss. Additionally, our investigation has been limited to the low-order model at equilibrium whereas the simulations in global climate models and the equivalent experiment being performed in nature have many more degrees of freedom, are forced by time-varying greenhouse gas levels, and are out of equilibrium. This raises the question of whether bifurcations in summer sea ice could be detected from a time series of sea ice in a GCM or in nature, and if so, what the implications would be. Previous attempts to detect bifurcations in climate time series have generally focused on characteristic slowing down of fluctuations as the bifurcation point is approached, related to the linear decay rate going to zero at a bifurcation [e.g., *Held and Kleinen*, 2004; *Livina and Lenton*, 2007; *Dakos et al.*, 2008; *Thompson and Sieber*, 2011]. Full consideration of this issue is beyond the scope of the current work, but as an initial step in the direction of understanding the issue we will simply consider the response of the low-order model to time-varying greenhouse gas forcing here.

[27] For illustrative purposes, we consider a simplified version of the low-order model with $\Delta A_c = 0$ W m^{-2}, $\Delta\alpha_c = 0.3$, ν = 0 yr^{-1}, F_b = 0 W m^{-2}, α_i = 0.6, α_o = 0.1, and B = 2.0 W m^{-2} K^{-1}. With these parameter values the model loses summer sea ice through bifurcations with h_a = 0.1 m, but

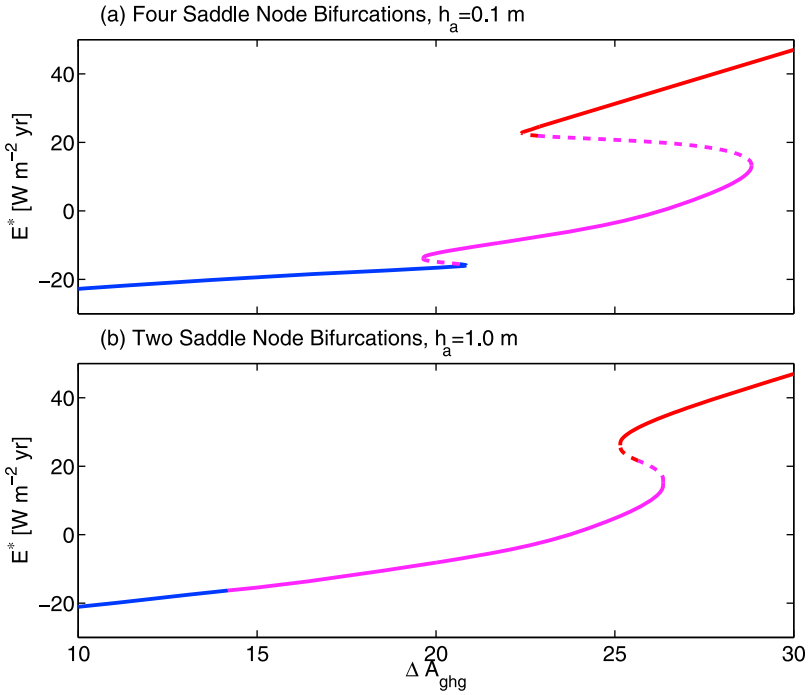

Figure 6. Typical bifurcation diagrams, computed from a Poincaré map associated with equation (2), showing energy on 1 January (E^*) as a function of ΔA_{ghg}. Model parameters used here are described in section 5. Parameters are chosen so that there are (a) four total saddle node bifurcations when $h_a = 0.1$ m and (b) two total saddle node bifurcations when $h_a = 1$ m. Stable fixed points of the map appear as solid lines and unstable fixed points appear as dashed lines. A blue curve indicates that the state is perennially ice covered ($E < 0$ throughout the seasonal cycle). A magenta curve indicates that the state is seasonally ice covered ($E < 0$ and $E > 0$ at different phases in the seasonal cycle). A red curve indicates that the state is ice free ($E > 0$ throughout the year).

does not for $h_a = 1.0$ m (Figure 6). The model loses winter sea ice through bifurcations for both $h_a = 0.1$ m and $h_a = 1.0$ m (Figure 6). For both values of h_a we choose a value of ΔA_{ghg} such that the winter ice thickness is approximately 3 m and the summer ice thickness is approximately 1 m. We then increase ΔA_{ghg} at a constant rate of $\frac{d\Delta A_{ghg}}{dt} = 0.1$ W m^{-2} yr^{-1}, a value that causes winter sea ice to be completely lost in roughly the same amount of time as the global climate models that lose winter sea ice in the Intergovernmental Panel on Climate Change (IPCC)'s CO_2 increase 1% yr^{-1} to quadrupling simulation [*Winton*, 2006].

[28] The resulting time series of ice thickness and system energy are shown in Figure 7. For both values of h_a there is a rapid decrease in winter ice thickness to zero when it drops below ~1 m, caused by crossing a saddle node bifurcation. If we saw such a time series in output from a global climate model, we might suspect that it was associated with a bifurcation. In contrast, when summer sea ice is lost through a bifurcation, the drop in ice thickness is small and it would likely be difficult to distinguish from the smooth summer sea ice loss case using the summer sea ice time series alone. This is because, in contrast to the winter situation, the bifurcation occurs when summer sea ice has a thickness that is near zero. This means that much of the jump in energy associated with crossing the saddle node bifurcation increases the ocean temperature rather than decreasing the ice thickness. The jump in energy as the system crosses a saddle node bifurcation in summer sea ice does, however, cause a large drop in winter sea ice thickness that can be clearly differentiated from the smooth transition case. This is because the winter sea ice thickness is far from zero when the bifurcation occurs.

[29] This preliminary investigation of the low-order model with time-varying greenhouse gas forcing suggests two possible things to look for when investigating whether global climate models exhibit bifurcations during summer sea ice loss. First, instead of looking for jumps in ice thickness, it appears that it may be useful to look for jumps in a diagnostic similar to the energy of the low-order model that combines ice thickness and ocean temperature. Second, somewhat counterintuitively, it may be useful to look for rapid declines in winter sea ice thickness as a sign of a bifurcation in summer sea ice. An added motivation for more thoroughly investigating the second observation is that large decreases in winter sea ice thickness, associated with complete loss of summer sea ice, have previously been used to argue that summer sea ice loss was *not* associated with a bifurcation [*Holland et al.*, 2008; *Notz*, 2009].

6. Discussion and Conclusion

[30] We have demonstrated a variety of bifurcation behavior in summer sea ice in a low-order model of Arctic climate and sea ice, depending on the changes in cloud albedo, cloud optical thickness, and heat transport as sea ice is lost. Is there evidence for such behavior in more com-

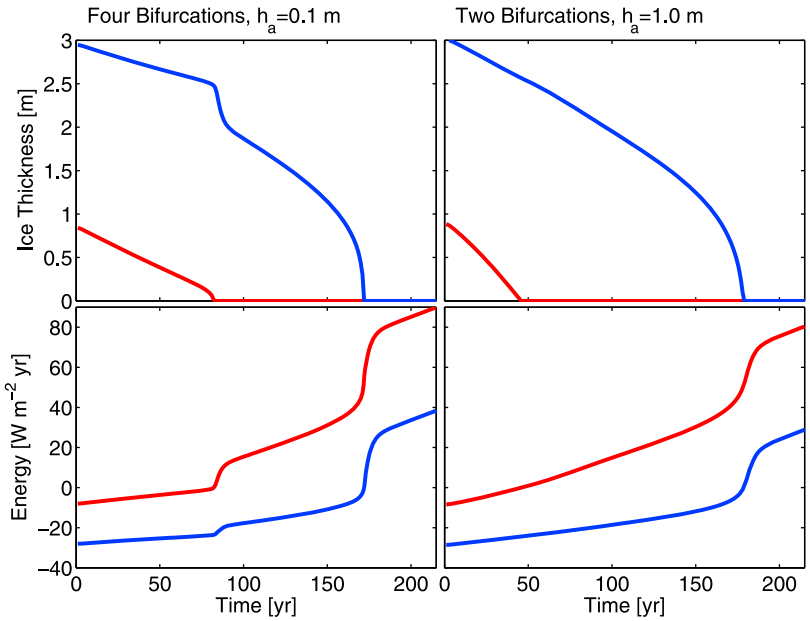

Figure 7. Time series of (top) ice thickness and (bottom) system energy in the low-order model when it is integrated with a linearly increasing ΔA_{ghg}($d\Delta A_{ghg}/dt$ = 0.1 W m^{-2} yr^{-1}). Blue curves indicate winter ice thickness or energy, and red curves indicate summer ice thickness or energy. (left) Summer sea ice is lost through saddle node bifurcations and h_a = 0.1 m (for four total bifurcations). (right) Summer sea ice is lost smoothly without bifurcations and h_a = 1.0 m (for two total bifurcations). Winter sea ice is lost through saddle node bifurcations in both cases.

plex GCMs? On the one hand, abrupt transitions in which September sea ice is lost throughout most of the Arctic, remaining only in certain coastal areas, as greenhouse gas levels are increased have been observed in roughly half of available GCMs, depending on the greenhouse gas forcing scenario [*Holland et al.*, 2006], which could be viewed as consistent with our result that the transition from perennial to seasonal sea ice coverage can be either smooth or abrupt, depending on model parameters. These transitions, however, were later interpreted as resulting more from intrinsically high variability of thin sea ice, than from bifurcation behavior [*Holland et al.*, 2008], although the work of *Merryfield et al.* [2008] suggests that the transitions could in fact have been associated with bifurcations. A similar study found extremely rapid loss of September sea ice suggestive of a tipping point in one (Centre National de Recherches Météorologiques (CNRM)) of six GCMs that provide a reasonable simulation of the observed sea ice record [*Wang and Overland*, 2009]. In a different test, *Tietsche et al.* [2011] found that Arctic summer sea recovers quickly to unperturbed values after it is set to zero during 21st century simulations in the Max-Planck-Institut (MPI) model, suggesting a lack of hysteresis in this model. Finally, some simulations shown by *Holland et al.* [2006] appear to exhibit jumping back and forth between low September Arctic sea ice coverage (3–5 × 10^6 km^2) and virtually no (<10^6 km^2) September Arctic sea ice, which is consistent with stochastic forcing of a system with coexisting stable perennial and seasonal ice states. These results indicate that many GCMs do not show strong signs of bifurcation behavior as summer sea ice is lost, although some appear to. This is consistent with our results that a bifurcation in summer sea ice loss would depend on model parameters and, if it exists, would be associated with a relatively small jump in the state of the system and relatively small hysteresis.

[31] More generally, determination of whether bifurcations in summer sea ice occur in GCMs may be difficult, given large climate noise and the potential that GCMs are being forced nonquasistatically. For example, despite the fact that both our model and the EW09 model predict a bifurcation as winter sea ice is lost in a wide parameter range, *Winton* [2006] found strong evidence for such a bifurcation in only one of two models analyzed. This could have to do with either the limitations of low-order models or the difficulty in choosing an appropriate metric to determine whether bifurcations occur in a GCM. Additionally, the work of *Merryfield et al.* [2008] suggests that climate noise may be obscuring the detection of bifurcations in summer sea ice loss in GCMs. This suggests that a thorough investigation of the time-varying greenhouse gas situation (section 5) should involve the addition of some sort of noise term, perhaps autoregressive, to equation (2) that would simulate climate noise. Finally, we note that our work would still raise the possibility of bifurcation behavior in summer sea ice in nature, even if it were definitively shown that such behavior does not occur in current GCMs.

[32] Our model is different from that of EW09; however, the seasonal ice state appears via a saddle node bifurcation in the EW09 model as well if a ΔA_c of 5 W m^{-2} is included (Figure 8). Similar behavior occurs in the EW09 model run with standard parameters if their h_α (our h_a) is decreased (Figure 9) (I. Eisenman, Factors controlling the bifurcation structure of sea ice retreat, submitted to *Journal of Geophysical Research*, 2011). Therefore, similar to the model of

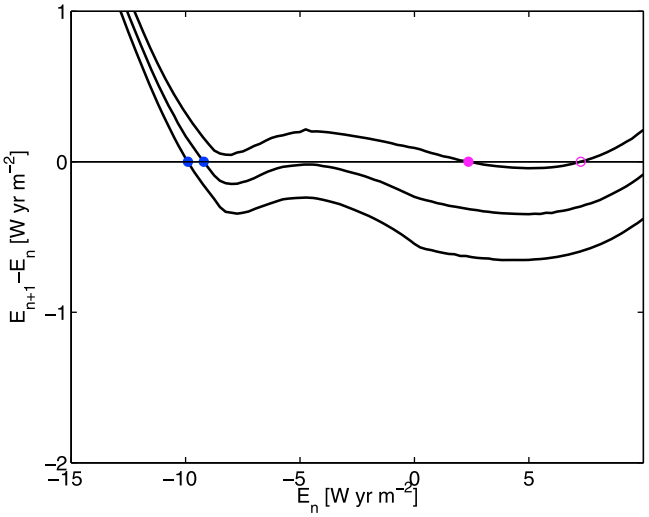

Figure 8. Poincaré map produced using the EW09 model with their standard parameters but with a ΔA_c of 5 W m^{-2} included. ΔA_c is subtracted from F_0 (EW09 notation) in the EW09 code using the formulation given in equation (5). Figure 8 focuses on the transition between perennial and seasonal ice coverage. Fixed points are colored as in Figures 3 and 4. ΔF_0 (EW09 notation) is 20.25, 20.5, and 20.75 W m^{-2} for the lines plotted here. A saddle node bifurcation produces and destroys the seasonal ice state, so that the system exhibits four total bifurcations, as in region II of Figure 5. The hysteresis in ΔF_0 associated with the transition from perennial to seasonal ice coverage is small (only ~0.25 W m^{-2}), but the January energy jumps ~10 W yr m^{-2} during this transition (the equivalent of ~1 m ice).

Merryfield et al. [2008], bifurcations may be associated with summer sea ice loss in both our model and that of EW09 in at least some parameter regime. This implies that these conceptual models should not be used to argue that such behavior is physically inconsistent.

[33] Some recent studies have indicated that the cloud feedback in the Arctic is negative [*Soden et al.*, 2008; *Boe et al.*, 2009; *Screen and Simmonds*, 2010]. If we assume that clouds increase the albedo by $\Delta\alpha_c^i$ when there is sea ice, then the total change in cloud radiative forcing from the ice-covered to the ice-free state in our model is $\Delta CRF = \Delta A_c + (\Delta\alpha_c^i - \Delta\alpha_c)\overline{F_s(t)}$. $\overline{F_s(t)}$ = 183.4 W m^{-2} when averaged north of 70.0°N, so that if we assume, for illustrative purposes, that $\Delta\alpha_c^i \approx 0.1$, we find that $\Delta CRF \approx -21$ W m^{-2} for NCEP/NCAR and $\Delta CRF \approx -29$ W m^{-2} for CAM. This indicates that the cloud feedback is negative in the potentially relevant areas of parameter space that we identified.

[34] As noted in section 4, $\Delta A_c = 0$ and $\Delta\alpha_c \approx 0.1$ in the study by EW09, which would yield $\Delta CRF \approx 0$. It might appear unsettling that our model incorporates what amounts to a negative, stabilizing cloud feedback that is not included in the EW09 model, yet we find less smooth behavior of summer sea ice. One relevant response to this concern is that, as noted above, loss of summer sea ice through bifurcations is possible in the EW09 model if h_a is decreased. Furthermore, we note again that direct comparison between our results and those of EW09 at specific parameter values is not possible given differences in model formulation (see section 4), such as the fact that EW09 assume a seasonal cycle in a number of model variables based on the modern perennially ice-covered Arctic and we do not (section 2). This underscores the fact that low-order models such as the one used here and that of EW09 should be used for conceptual understanding rather than for specific predictions. In this context, our main result is that loss of seasonal sea ice in such models is possible in a seemingly reasonable region of parameter space.

[35] Eisenman (submitted manuscript, 2011) argues that although bifurcations are possible as summer sea ice is lost in single column models, they are likely artifacts of reduced dimensionality in such models. This argument highlights the vast chasm between low-dimensional models, such as the one used here, and IPCC class global climate models. Furthermore, it suggests that work filling this gap in model hierarchy would be essential to increase understanding. It would be useful, for example, to determine whether bifurcations leading to summer sea ice loss are possible in a one-dimensional energy balance model with thermodynamic sea ice. Such a model would also help us to determine a reasonable value of h_a in the low-order model used in this paper. h_a, which accounts for spatial heterogeneity in sea ice loss, is crucial for determining model bifurcation behavior (section 4), and is essentially unconstrained in the low-order model.

[36] To conclude, by including additional physical effects and doing a complete exploration of parameter space, we find an expanded range of potential sea ice loss bifurcation behavior compared with EW09, including the possibility of

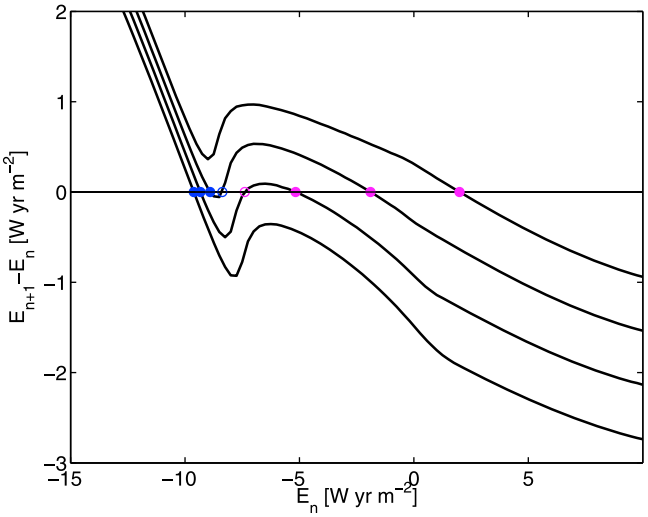

Figure 9. Poincaré map produced using the EW09 model with their standard parameters but with h_α = 0.1 m (EW09 notation). Figure 9 focuses on the transition between perennial and seasonal ice coverage. Fixed points are colored as in Figures 3 and 4. ΔF_0 (EW09 notation) is 25, 25.5, 26, and 26.5 W m^{-2} for the lines plotted here. Figure 9 demonstrates that the transition to seasonal ice occurs via a saddle node bifurcation in the EW09 model run with standard parameters even without changing ΔA_c or $\Delta\alpha_c$, if the width of the albedo transition zone is decreased.

loss of summer sea ice through saddle node bifurcations. We note, however, that when the seasonal ice state is created and destroyed by saddle node bifurcations, we find that the jump in energy and hysteresis in greenhouse gas variations associated with loss of winter sea ice are both larger than those associated with loss of summer sea ice. Therefore, consistent with the general theme of EW09 and the review of *Notz* [2009], we find that nonlinear behavior is more likely and would likely be stronger for winter sea ice loss than summer sea ice loss.

Appendix A: Seasonal Ice State Existence Boundary

[37] The boundary in the ($\Delta\alpha_c$, ΔA_c) parameter plane of Figure 5 that determines the existence region for seasonal ice states is approximately a straight line. Analysis of equation (2) yields conditions for this line to be straight. Since the boundary between regions II and III is roughly independent of the value of h_a, we can derive a formula for its slope by considering the limit $h_a \to 0$. In this case, the ice-free phase ($E \geq 0$) of the seasonal cycle, between the melting time t_m and refreezing times t_f, which are unknown a priori, is governed by the linear differential equation

$$\frac{dE}{dt} + \frac{B}{C_s}E = (1 - \alpha_o - \Delta\alpha_c)F_s(t) - \left(A_0 - F_{south} - F_b - \Delta A_c - \Delta A_{ghg}\right). \quad \text{(A1)}$$

After multiplication by the integrating factor $e^{\frac{C_s}{}}$, we find

$$\frac{d}{dt}\left(e^{\frac{B}{C_s}t}E\right) = (1 - \alpha_o - \Delta\alpha_c)F_s(t)e^{\frac{B}{C_s}t} - \left(A_0 - F_{south} - F_b - \Delta A_c - \Delta A_{ghg}\right)e^{\frac{B}{C_s}t}. \quad \text{(A2)}$$

We integrate equation (A2) from $t = t_m$ to $t = t_f$ and exploit the fact that $E(t_m) = E(t_f) = 0$ to obtain the following equation that relates the melting and freezing times to the other parameters of the problem

$$\frac{\int_{t_m}^{t_f} F_s(t)e^{Bt/C_s}dt}{\left(e^{Bt_f/C_s} - e^{Bt_m/C_s}\right)C_s/B} = \frac{\left(A_0 - F_{south} - F_b - \Delta A_c - \Delta A_{ghg}\right)}{(1 - \alpha_o - \Delta\alpha_c)}. \quad \text{(A3)}$$

A second, more complicated, implicit equation for t_m and t_f is obtained by solving the nonlinear differential equation that applies during the sea ice phase of the cycle, when $E < 0$. This second relation is independent of both $\Delta\alpha_c$ and ΔA_c in the limit $h_a \to 0$, therefore these parameters only affect the solution through equation (A3). For the line that separates regions II and III in Figure 5 to be straight, variations in ΔA_{ghg} must be negligible compared to variations in $\Delta\alpha_c$ and ΔA_c. Our numerical integrations suggest that this is in fact the case, which allows us to use equation (A3) to calculate the value of the slope of this line. Using values of ($\Delta\alpha_c$, ΔA_c, A_{ghg}) at one point on the line we find a slope that is in excellent agreement with the value obtained numerically (Figure 5).

[38] **Acknowledgments.** We thank Ian Eisenman for helpful comments. D.S.A. was supported by the T. C. Chamberlin Fellowship of the University of Chicago and the Canadian Institute for Advanced Research. M.S. was supported by NSF DMS-0929419.

References

Abbot, D. S., C. C. Walker, and E. Tziperman (2009a), Can a convective cloud feedback help to eliminate winter sea ice at high CO_2 concentrations?, *J. Clim.*, *22*(21), 5719–5731, doi:10.1175/2009JCLI2854.1.

Abbot, D. S., M. Huber, G. Bousquet, and C. C. Walker (2009b), High-CO_2 cloud radiative forcing feedback over both land and ocean in a global climate model, *Geophys. Res. Lett.*, *36*, L05702, doi:10.1029/2008GL036703.

Bitz, C. M., P. R. Gent, R. A. Woodgate, M. M. Holland, and R. Lindsay (2006), The influence of sea ice on ocean heat uptake in response to increasing CO_2, *J. Clim.*, *19*(11), 2437–2450, doi:10.1175/JCLI3756.1.

Boe, J., A. Hall, and X. Qu (2009), Current GCMs' unrealistic negative feedback in the Arctic, *J. Clim.*, *22*(17), 4682–4695, doi:10.1175/2009JCLI2885.1.

Dakos, V., M. Scheffer, E. H. van Nes, V. Brovkin, V. Petoukhov, and H. Held (2008), Slowing down as an early warning signal for abrupt climate change, *Proc. Natl. Acad. Sci. U. S. A.*, *105*(38), 14,308–14,312, doi:10.1073/pnas.0802430105.

Eisenman, I., and J. S. Wettlaufer (2009), Nonlinear threshold behavior during the loss of Arctic sea ice, *Proc. Natl. Acad. Sci. U. S. A.*, *106*(1), 28–32, doi:10.1073/pnas.0806887106.

Fetterer, F., K. Knowles, W. Meier, and M. Savoie (2002), Sea ice index, http://nsidc.org/data/seaice_index, Natl. Snow and Ice Data Cent., Boulder, Colo. [Updated 2009.]

Held, H., and T. Kleinen (2004), Detection of climate system bifurcations by degenerate fingerprinting, *Geophys. Res. Lett.*, *31*, L23207, doi:10.1029/2004GL020972.

Holland, M. M., C. M. Bitz, and B. Tremblay (2006), Future abrupt reductions in the summer Arctic sea ice, *Geophys. Res. Lett.*, *33*, L23503, doi:10.1029/2006GL028024.

Holland, M. M., C. M. Bitz, B. Tremblay, and D. A. Bailey (2008), The role of natural versus forced change in future rapid summer Arctic ice loss, in *Arctic Sea Ice Decline: Observations, Projections, Mechanisms, and Implications*, *Geophys. Monogr. Ser.*, vol. 180, edited by E. T. DeWeaver, C. M. Bitz, and B. Tremblay, pp. 133–150, AGU, Washington, D. C.

Huybers, P., and I. Eisenman (2006), Integrated summer insolation calculations, http://www.ncdc.noaa.gov/paleo/forcing.html, World Data Cent. for Paleoclimatol., Boulder, Colo.

Kalnay, E., et al. (1996), The NCEP/NCAR 40-year reanalysis project, *Bull. Am. Meteorol. Soc.*, *77*(3), 437–471.

Kay, J. E., and A. Gettelman (2009), Cloud influence on and response to seasonal Arctic sea ice loss, *J. Geophys. Res.*, *114*, D18204, doi:10.1029/2009JD011773.

Kay, J. E., T. L'Ecuyer, A. Gettelman, G. Stephens, and C. O'Dell (2008), The contribution of cloud and radiation anomalies to the 2007 Arctic sea ice extent minimum, *Geophys. Res. Lett.*, *35*, L08503, doi:10.1029/2008GL033451.

Lindsay, R. W., and J. Zhang (2005), The thinning of Arctic sea ice, 1988–2003: Have we passed a tipping point?, *J. Clim.*, *18*(22), 4879–4894, doi:10.1175/JCLI3587.1.

Livina, V. N., and T. M. Lenton (2007), A modified method for detecting incipient bifurcations in a dynamical system, *Geophys. Res. Lett.*, *34*, L03712, doi:10.1029/2006GL028672.

McBean, G., G. Alekseev, D. Chen, E. Forland, J. Fyfe, P. Y. Groisman, R. King, H. Melling, R. Vose, and P. H. Whitfield (2005), Arctic climate: Past and present, in *Arctic Climate Impact Assessment*, edited by C. Symon, L. Arris, and B. Heal, pp. 22–60, Cambridge Univ. Press, Cambridge, U. K.

Merryfield, W. J., M. M. Holland, and A. H. Monahan (2008), Multiple equilibria and abrupt transitions in Arctic summer sea ice extent, in *Arctic Sea Ice Decline: Observations, Projections, Mechanisms, and Implications*, *Geophys. Monogr. Ser.*, vol. 180, edited by E. T. DeWeaver, C. M. Bitz, and B. Tremblay, pp. 151–174, AGU, Washington, D. C.

North, G. R. (1975), Analytical solution to a simple climate model with diffusive heat transport, *J. Atmos. Sci.*, *32*(7), 1301–1307.

North, G. R. (1984), The small ice cap instability in diffusive climate models, *J. Atmos. Sci.*, *41*(23), 3390–3395.

Notz, D. (2009), The future of ice sheets and sea ice: Between reversible retreat and unstoppable loss, *Proc. Natl. Acad. Sci. U. S. A.*, *106*(49), 20,590–20,595, doi:10.1073/pnas.0902356106.

Pierrehumbert, R. T. (2002), The hydrologic cycle in deep-time climate problems, *Nature*, *419*(6903), 191–198, doi:10.1038/nature01088.

Schweiger, A. J., R. W. Lindsay, S. Vavrus, and J. A. Francis (2008), Relationships between Arctic sea ice and clouds during autumn, *J. Clim.*, *21*(18), 4799–4810, doi:10.1175/2008JCLI2156.1.

Screen, J. A., and I. Simmonds (2010), The central role of diminishing sea ice in recent arctic temperature amplification, *Nature*, *464*(7293), 1334–1337, doi:10.1038/nature09051.

Soden, B. J., and I. M. Held (2006), An assessment of climate feedbacks in coupled ocean–atmosphere models, *J. Clim.*, *19*(14), 3354–3360, doi:10.1175/JCLI3799.1.

Soden, B. J., I. M. Held, R. Colman, K. M. Shell, J. T. Kiehl, and C. A. Shields (2008), Quantifying climate feedbacks using radiative kernels, *J. Clim.*, *21*(14), 3504–3520, doi:10.1175/2007JCLI2110.1.

Strogatz, S. H. (1994), *Nonlinear Dynamics and Chaos: With Applications to Physics, Biology, Chemistry, and Engineering*, Addison-Wesley, Reading, Mass.

Thompson, J., and J. Sieber (2011), Climate tipping as a noisy bifurcation: A predictive technique, *IMA J. Appl. Math.*, *76*(1), 27–46.

Tietsche, S., D. Notz, J. H. Jungclaus, and J. Marotzke (2011), Recovery mechanisms of Arctic summer sea ice, *Geophys. Res. Lett.*, *38*, L02707, doi:10.1029/2010GL045698.

Vavrus, S., D. Waliser, A. Schweiger, and J. Francis (2009), Simulations of 20th and 21st century Arctic cloud amount in the global climate models assessed in the IPCC AR4, *Clim. Dyn.*, *33*, 1099–1115, doi:10.1007/s00382-008-0475-6.

Wang, M., and J. E. Overland (2009), A sea ice free summer Arctic within 30 years?, *Geophys. Res. Lett.*, *36*, L07502, doi:10.1029/2009GL037820.

Winton, M. (2006), Does the Arctic sea ice have a tipping point?, *Geophys. Res. Lett.*, *33*, L23504, doi:10.1029/2006GL028017.

D. S. Abbot and R. T. Pierrehumbert, Department of Geophysical Sciences, University of Chicago, Chicago, IL 60637, USA. (abbot@uchicago.edu)

M. Silber, Department of Engineering Sciences and Applied Mathematics, Northwestern University, Evanston, IL 60208, USA.